INTERNATIONAL JOURNAL FOR NUMERICAL METHODS IN FLUIDS
Int. J. Numer. Meth. Fluids 2008; **57**:93–117
Published online 11 October 2007 in Wiley InterScience (www.interscience.wiley.com). DOI: 10.1002/fld.1627

Generation of turbulent inflow and initial conditions based on multi-correlated random fields

M. Fathali[1,*,†], M. Klein[2], T. Broeckhoven[3], C. Lacor[3] and M. Baelmans[1]

[1]*Department of Mechanical Engineering, K.U. Leuven, Celestijnenlaan 300 A, 3001 Heverlee, Belgium*
[2]*Department of Energy and Powerplant Technology, TU Darmstadt, Petersenstrasse 30, 64287 Darmstadt, Germany*
[3]*Department of Mechanical Engineering, Vrije Universiteit Brussel, Pleinlaan 2, 1050 Brussel, Belgium*

SUMMARY

Direct or large eddy simulation of a turbulent flow field is strongly influenced by its initial or inflow boundary condition. This paper presents a new stochastic approach to generate an artificial turbulent velocity field for initial or inflow boundary condition based on digital filtering. Each velocity component of the artificial turbulent velocity field is generated by linear combination of individual uncorrelated random fields. These uncorrelated random fields are obtained by filtering random white-noise fields. Using common elements in these linear combinations results in multi-correlation among different velocity components. The generated velocity field reproduces locally desired Reynolds stress components and integral length scales including cross-integral length scales. The method appears to be simple, flexible and more accurate in comparison with previously developed methods. The accuracy and performance of the method are demonstrated by numerical simulation of a homogeneous turbulent shear flow with high and low shear rates. To assess the accuracy and performance of the method, simulation results are compared with a reference simulation. Copyright © 2007 John Wiley & Sons, Ltd.

Received 19 December 2006; Revised 12 August 2007; Accepted 24 August 2007

KEY WORDS: turbulent inflow and initial condition generation; stochastic method; DNS; LES; digital filtering

1. INTRODUCTION

The increasing performance of current computer technology makes the numerical simulation of turbulent flows using direct numerical simulation (DNS) and large eddy simulation (LES) techniques attractive. These approaches are able to describe the flow features that cannot be handled

*Correspondence to: M. Fathali, Department of Mechanical Engineering, K.U. Leuven, Celestijnenlaan 300 A, 3001 Heverlee, Belgium.
†E-mail: Mani.Fathali@mech.kuleuven.be, mani.fathali@gmail.com

Contract/grant sponsor: FWO-Vlaanderen

with Reynolds-averaged Navier–Stokes (RANS) simulations such as significant unsteadiness and dynamics of the coherent structures (CS) as well as information about higher moment statistics.

Since in these approaches more flow-field structures are captured, their upstream or initial information must also be specified at inflow boundaries of the computational domain or as initial condition. In other words, in contrast to RANS methods where only mean profiles or one-point flow-field statistics, such as k, ε or Reynolds stresses, must be prescribed, in DNS and LES all the resolved scales must be quantified. Therefore, one of the critical issues in DNS and LES is a realistic prescription of these conditions, able to mimic the main features of an actual turbulent flow. This issue is generally denoted as *supergrid* modeling [1].

Two particular problems make *supergrid* modeling a difficult task. One problem is the prolongation of the required computational domain or time to develop a realistic turbulent field from inappropriate perturbations. The other serious problem is the large influence of this modeling on the long term or asymptotic state of the flow-field development [2]. Owing to the chaotic character of the Navier–Stokes (NS) equations, any uncertainty in inflow or initial condition can remain as a source of error during the simulation and strongly affect the afterward flow-field development [3–9]. Although it is not completely clear, it is mainly believed that this profound effect of upstream or initial conditions on the turbulent flow-field development is largely influenced by the characters of CS [9–11]. Therefore, correct specifications of these flow-field structures at inflow or as initial condition is a critical issue in *supergrid* modeling.

As a solution, an auxiliary simulation prior or parallel to the main simulation can be carried out to provide exact flow-field information. On the basis of this exact information, either the complete flow field or only the CS can be reconstructed at the inflow or as initial condition. Although this technique provides satisfactory results, its application can be extremely expensive [9, 12–14]. Therefore, using indeterministic or stochastic approaches to reconstruct these data with a plausible level of approximation and computational cost, have been extensively investigated as an alternative.

In stochastic approaches, turbulent inflow or initial conditions are random realizations that are statistically equivalent with an actual turbulent flow field. However, in practice, the imposed statistical information is often limited to the correlation function $R_{ij}(\mathbf{x}, \mathbf{r})$, which contains a great deal of information [15, 16]. Instead of the huge amount of information contained in the correlation function, a lower level of statistical description provided by different related quantities is mostly considered. Depending on the candidate statistical quantities, such as Reynolds stresses, energy spectra, a variety of stochastic methods have emerged [12, 17–23].

Lee *et al.* [17] proposed a method, based on the appropriate rescaling of a random white-noise field in wave number space, to generate a turbulent velocity field with prescribed energy spectrum [24]. This quantity provides a simpler although less complete description for the correlation function, i.e. all the directional and phase information is lost and has to be reconstructed randomly. The generated turbulent velocity field does not show specific correlation between different velocity components in general. However, in this method, the energy content of the CS can be specified through an energy spectrum function over the low wave number part of the energy spectrum. Moreover, the incompressible kinematic constraint for a turbulent velocity field, i.e. divergence-free velocity field, can be easily applied through a projection method in wave number space. Finally, since this procedure is based on Fourier transformation of the velocity field, its application is restricted to simple geometries with homogeneous directions.

Hoshiya [25] and Shinozuka [26] developed a procedure to generate multi-correlated random fields based on the prescribed correlation function, which was later extended to a variety of

DOI: 10.1002/fld

methods. The main idea is to generate a set of correlated random data by a linear transformation from a set of uncorrelated random data. The kernel of this linear transformation is obtained from decomposition of the target correlation function matrix. The generated turbulent field based on this approach can have correct correlation for all velocity components. Using the space–time correlation function instead of space correlation, this approach is able to introduce time correlation to the generated random velocity field [18, 23]. Although these procedures are able to generate random turbulent fields which are statistically identical with an actual turbulent flow, their application is limited by the extremely huge amount of required information and computational load.

Lund *et al.* [12] proposed a method to generate a turbulent velocity field with prescribed mean profile and Reynolds stresses. In this method, instead of the correlation function, the Reynolds stress tensor is decomposed as the kernel for the transformation. Although this one-point statistic information is easily available for most of the cases, direct control on the CS during flow-field generation based on this procedure is not possible and the generated velocity field shows a flat energy spectrum, i.e. white noise, which is the main drawback of this method [9].

Smirnov *et al.* [22] modified the Fourier modes scaling procedure of Lee *et al.* [17] by applying Lund's transformation on a continuous flow field generated as a superposition of harmonic functions. Scaling of the arguments of these harmonic functions based on the flow-field characteristic length and time scales allows one to introduce anisotropy of turbulence. Consequently, the outcome is a time-dependent flow field with prescribed Reynolds stresses and prespecified turbulent characteristic time and length scales. This improvement, allows a crude description of CS through characteristic length scale and makes the method applicable to more complex flow fields.

Klein *et al.* [27] proposed a new procedure based on the digital filtering of random data followed by Lund's [12] transformation. This method is able to generate an artificial turbulent velocity field with prescribed Reynolds stresses. Moreover, the generated velocity field has a locally prescribed autocorrelation coefficient function. Introducing this second-order, two-point statistics in the generated flow field, increases the description level for the CS. With a further simplification, which is specially preferable from an application point of view, this method is able to satisfy local integral length scales instead of the autocorrelation function. Hereby, there is a more complete control on the specification of the CS during the generation procedure based on the exact available information from experiments or simulations or an intuitive feeling of flow-field length scales.

This method is further refined and extended by other authors [28, 29]. Kempf *et al.* [28] improved this method by replacing the filtering procedure with applying physical diffusion. In this method, by choosing an appropriate local diffusion coefficient, prescribed integral length scales are established. The generated random fields based on this method and digital filtering method [27] are equivalent, but the advantage of this method is its applicability to complex geometries and arbitrary computational grids. Mare *et al.* [29] further extended the digital filtering method [27] by locally computing filter functions based on the correlation tensor decomposition. This improvement increases the ability of the method to reproduce the complete Reynolds stress tensor as well as any given, locally defined, spatial and temporal correlation functions.

The great advantage of these recent methods is the ability to reproduce the most important features of a turbulent field, i.e. CS, based on easily available statistical information and within an acceptable computational cost. In these methods, first velocity components are generated by

DOI: 10.1002/fld

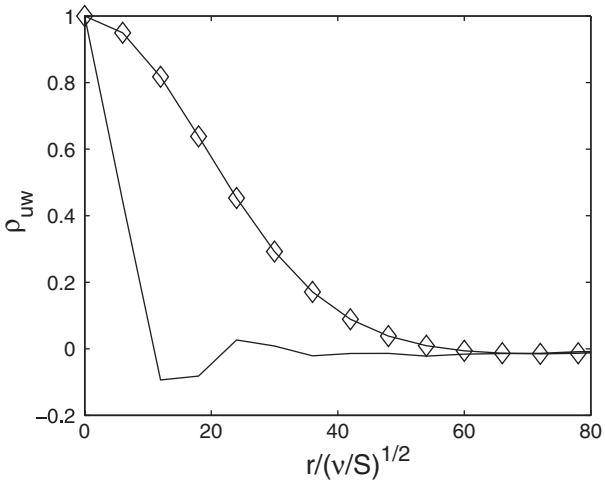

Figure 1. Cross-correlation coefficient function for a homogeneous turbulent shear flow with mean shear rate $S=15$ and $\nu=0.0035$ at well-developed stage. (—), reference flow-field correlation function; (—◇—), digital filtering method.

filtering (digital or based on the physical diffusion) white-noise fields to establish autocorrelation functions, i.e. R_{uu}, R_{vv} and R_{ww}, or their respective integral length scales. Subsequently, Lund's transformation combines these velocity components in such a way that the transformed velocity components yield correct Reynolds stresses.

Since in this method, Lund's transformation and filtering are performed in different steps, in flow fields with high anisotropy the exact autocorrelation function or its integral length scale, generated during the filtering step can be changed by the transformation. In addition, the resulting cross-correlations between different velocity components, established through Lund's transformation, can be significantly different from their physical value. This second issue can be clearly observed by considering a turbulent homogeneous shear flow with high shear rate. The velocity flow field of this flow at specific time is reconstructed based on the above-mentioned method. Figure 1 reveals that the cross-correlation function and consequently its related integral length scale established through Lund's transformation shows a huge difference from its physical value.

The objective of the present study is to complement the above-mentioned procedures, specifically the digital filtering method [27], concerning these two issues. A new method is presented, which generates a turbulent velocity field with exact prescribed Reynolds stresses and integral length scales including the cross-integral length scales between different velocity components thus leading to a more accurate description of the CS. The required statistical information for this method are Reynolds stresses and integral length scales of the flow field.

The importance of the cross-integral length scales can be better realized by considering the fact that the cross-spectra energy terms $\Phi_{ij}(\kappa)$ decay very fast with increasing wave number κ. It means that the main contribution to the $\Phi_{ij}(\kappa)$, and consequently Reynolds stresses $\langle u_i u_j \rangle$, comes from small κ or relevant large scales. Therefore, cross-integral length scale, as a measure for significant

DOI: 10.1002/fld

correlation between different velocity components, can have a profound effect on the Reynolds stresses and consequently on the turbulent production.

This paper is further organized as follows. First, the new methodology to generate a stochastic turbulent flow field with prescribed Reynolds stresses and integral scales is presented. Then the method is applied to a homogeneous turbulent shear flow and the influence of the level of statistical information introduced in the procedure is investigated. Finally, it is shown that the new method has a better overall performance.

2. IMPROVED APPROACH TO GENERATE ARTIFICIAL TURBULENCE

The conventional way to generate a stochastically turbulent velocity field is to superimpose velocity fluctuations to a mean flow velocity field. These velocity fluctuations are random fields with certain statistical properties, which may, for example, be known from experimental data. In this section, the new methodology for generating these fluctuating fields is explained and a procedure for the proposed method is given. To improve the readability of the paper, mathematical derivations are discussed in the Appendices.

2.1. Basic mathematical derivation

In this method a turbulent velocity field is generated with prescribed Reynolds stresses and integral length scales including the cross-integral length scales. The integral length scale can be considered as a statistical quantity providing a measure of the extent of the region where velocity components are significantly correlated and it is closely related to the correlation function

$$R_{ij}(\mathbf{x},\mathbf{r},t)=\langle u_i(\mathbf{x}+\mathbf{r},t)u_j(\mathbf{x},t)\rangle \tag{1}$$

between the i and j velocity components, separated by a distance vector $\mathbf{r}$. This two-point, one-time covariance is the simplest statistic containing some information on the spatial structure of a random field. From this quantity it is possible to define various integral length scales, e.g.

$$l_{ij}(\mathbf{x})=\int_0^\infty \frac{R_{ij}(\mathbf{x},r\mathbf{e})}{R_{ij}(\mathbf{x},0)}\,\mathrm{d}r=\frac{1}{\langle u_i u_j\rangle}\int_0^\infty \langle u_i(\mathbf{x})u_j(\mathbf{x}+r\mathbf{e})\rangle\,\mathrm{d}r \tag{2}$$

where $\mathbf{e}$ is the unit vector in an arbitrary direction, in practice x, y or z direction and $r=\sqrt{x^2+y^2+z^2}$.

From this definition it can be observed that the correlation functions and their respective integral length scales are functions of the separation direction $\mathbf{e}$. Moreover, the cross-integral length scales depend on the considered velocity components, separated by $r\mathbf{e}$, i.e. $\langle u_i(\mathbf{x})u_j(\mathbf{x}+r\mathbf{e})\rangle$ and $\langle u_i(\mathbf{x}+r\mathbf{e})u_j(\mathbf{x})\rangle$ are generally not identical.

Because of this, different integral length scales can be attributed to a turbulent velocity field, depending on the arguments used to compute the correlation function. This possibility to define different integral length scales increases the required statistical information and consequently the complexity of the proposed method which is not desirable from an application point of view.

As it will be explained, in the proposed method the flow field is generated based on filtering with a spherically symmetric filter function. Therefore, the established correlation functions and their

DOI: 10.1002/fld

respective integral length scales have spherical symmetries and do not depend on the separation direction **e**. With an implicit homogeneity assumption, cross-integral length scales become identical for different shifted velocity components and the level of complexity is further reduced. These simplifying assumptions make the definition of integral length scales unique. Therefore, for this method we can introduce only one quantity for each of the length scales l_{uu}, l_{vv}, l_{ww}, l_{uv}, l_{uw} and l_{vw}.

In the new method, a multi-correlated random velocity field is generated by combining different uncorrelated random fields f_{ij} with zero mean. Each velocity component u, v and w is formed by a linear combination of these fields, i.e.

$$\begin{aligned} u &= a_{11} f_{11} + a_{12} f_{12} + a_{13} f_{13} \\ v &= a_{21} f_{12} + a_{22} f_{22} + a_{23} f_{23} \\ w &= a_{31} f_{13} + a_{32} f_{23} + a_{33} f_{33} \end{aligned} \tag{3}$$

The presence of field f_{12} in u and v establishes a cross-correlation between these velocity components and the same is true for f_{13} (u and w) and f_{23} (v and w). It can be shown (see Appendix A) that the correlation functions for the obtained velocity field, described by Equation (3), are related to the autocorrelation functions of the individual random fields f_{ij} as follows:

$$\begin{aligned} R_{uu} &= (a_{11})^2 r_{11} + (a_{12})^2 r_{12} + (a_{13})^2 r_{13} \\ R_{vv} &= (a_{21})^2 r_{12} + (a_{22})^2 r_{22} + (a_{23})^2 r_{23} \\ R_{ww} &= (a_{31})^2 r_{13} + (a_{32})^2 r_{23} + (a_{33})^2 r_{33} \\ R_{uv} &= (a_{12})(a_{21}) r_{12} \\ R_{uw} &= (a_{13})(a_{31}) r_{13} \\ R_{vw} &= (a_{23})(a_{32}) r_{23} \end{aligned} \tag{4}$$

where R_{ij} are the correlation functions for the generated velocity components and r_{ij} are the autocorrelation functions of the initial random fields f_{ij}, e.g. $r_{12} = \langle f_{12}(\mathbf{x}) f_{12}(\mathbf{x}') \rangle$ where $\mathbf{x}' = \mathbf{x} + \mathbf{r}$.

In general, the set of Equations (4) contain nine unknown coefficients a_{ij} and six unknown correlation functions r_{ij} which must be determined from 12 quantities related to the known correlation functions R_{ij} (i.e. six integral length scales l_{ij} and six Reynolds stresses $\langle u_i u_j \rangle$). To make this possible, some simplifications are required. First, a specific shape is assumed for the six unknown correlation functions r_{ij} and secondly the number of unknown coefficients a_{ij} is reduced by assuming some relationship among them.

For the unknown correlation functions r_{ij} a gaussian shape is assumed, equivalent to the autocorrelation function of homogeneous isotropic turbulence in the final period of decay. With this assumption, theoretically, the spectral content of the generated velocity field is reasonable and consistent with the viscous structure of the NS equations [16, 24]. Moreover, a normalized gaussian function can be uniquely specified with one coefficient, i.e. its variance σ, thus reducing the problem to the determination of six unknown coefficients, σ_{ij}.

It can be shown that filtering an uncorrelated random field generates a correlation in the filtered field closely related to the filter function [27]. More specifically, by choosing a gaussian filter, the correlation function has also a gaussian shape with a variance related to the filter width [27, 28].

DOI: 10.1002/fld

Considering this property, each initial random uncorrelated field, f_{ij} in Equation (3), can be generated by applying a gaussian filter, with appropriate filter width, to a white-noise field ξ_{ij}:

$$f_{ij}(\mathbf{x}) = F_{ij} \circ \xi_{ij} = \int_{-\infty}^{+\infty} \xi_{ij}(\mathbf{x}') F_{ij}(\mathbf{x}, \mathbf{x}-\mathbf{x}')\, \mathrm{d}\mathbf{x}' \tag{5}$$

where $\circ$ denotes convolution and the filter function has a gaussian shape with spherical symmetry

$$F_{ij}(\mathbf{x}) = \exp\left(-\frac{r^2}{\sigma_{ij}^2}\right) \tag{6}$$

and σ_{ij} is the filter width which can be a function of spatial coordinate $\mathbf{x}$. Moreover, all the ξ_{ij} used in Equation (5) are mutually uncorrelated and have zero mean:

$$\langle \xi_{ij} \xi_{mn} \rangle = \delta_{im} \delta_{jn}, \quad \langle \xi_{ij} \rangle = 0 \tag{7}$$

A further simplification concerns reducing the nine unknown coefficients a_{ij} by assuming that in Equation (3) the cross-term coefficients a_{ij} and a_{ji} are established with a common structure f_{ij}. However, the sign of these cross-term coefficients depend on the sign of the respective Reynolds stresses. This leads to

$$a_{ij} = \mathrm{sign}(\langle u_i u_j \rangle).a_{ji} = \pm a_{ji} \tag{8}$$

where $\mathrm{sign}(\langle u_i u_j \rangle)$ is the sign of the Reynolds stress components, $\langle u_i u_j \rangle$:

$$\mathrm{sign}(\langle u_i u_j \rangle) = \frac{\langle u_i u_j \rangle}{|\langle u_i u_j \rangle|} = \pm 1 \tag{9}$$

With these assumptions the following set of equations for the generated velocity field is obtained:

$$\begin{aligned}
u &= a_{11} \exp\left(-\frac{r^2}{\sigma_{11}^2}\right) \circ \xi_{11} + a_{12} \exp\left(-\frac{r^2}{\sigma_{12}^2}\right) \circ \xi_{12} + a_{13} \exp\left(-\frac{r^2}{\sigma_{13}^2}\right) \circ \xi_{13} \\
v &= \pm a_{12} \exp\left(-\frac{r^2}{\sigma_{12}^2}\right) \circ \xi_{12} + a_{22} \exp\left(-\frac{r^2}{\sigma_{22}^2}\right) \circ \xi_{22} + a_{23} \exp\left(-\frac{r^2}{\sigma_{23}^2}\right) \circ \xi_{23} \\
w &= \pm a_{13} \exp\left(-\frac{r^2}{\sigma_{13}^2}\right) \circ \xi_{13} \pm a_{23} \exp\left(-\frac{r^2}{\sigma_{23}^2}\right) \circ \xi_{23} + a_{33} \exp\left(-\frac{r^2}{\sigma_{33}^2}\right) \circ \xi_{33}
\end{aligned} \tag{10}$$

where $+$ or $-$ for some coefficients in v and w components in Equation (10) are determined based on the signs of related Reynolds stresses $\langle u_i u_j \rangle$, i.e. *via* Equation (9). Correlation functions for

DOI: 10.1002/fld

the generated velocity field expressed by Equation (10) are (see Appendix B for more details):

$$
\begin{aligned}
R_{uu} &= \left(a_{11}^2\sqrt{\frac{\pi}{2}}\sigma_{11}\right)\exp\left(-\frac{r^2}{2\sigma_{11}^2}\right)+\left(a_{12}^2\sqrt{\frac{\pi}{2}}\sigma_{12}\right)\exp\left(-\frac{r^2}{2\sigma_{12}^2}\right)\\
&\quad+\left(a_{13}^2\sqrt{\frac{\pi}{2}}\sigma_{13}\right)\exp\left(-\frac{r^2}{2\sigma_{13}^2}\right)\\
R_{vv} &= \left(a_{12}^2\sqrt{\frac{\pi}{2}}\sigma_{12}\right)\exp\left(-\frac{r^2}{2\sigma_{12}^2}\right)+\left(a_{22}^2\sqrt{\frac{\pi}{2}}\sigma_{22}\right)\exp\left(-\frac{r^2}{2\sigma_{22}^2}\right)\\
&\quad+\left(a_{23}^2\sqrt{\frac{\pi}{2}}\sigma_{23}\right)\exp\left(-\frac{r^2}{2\sigma_{23}^2}\right)\\
R_{ww} &= \left(a_{13}^2\sqrt{\frac{\pi}{2}}\sigma_{13}\right)\exp\left(-\frac{r^2}{2\sigma_{13}^2}\right)+\left(a_{23}^2\sqrt{\frac{\pi}{2}}\sigma_{23}\right)\exp\left(-\frac{r^2}{2\sigma_{23}^2}\right)\\
&\quad+\left(a_{33}^2\sqrt{\frac{\pi}{2}}\sigma_{33}\right)\exp\left(-\frac{r^2}{2\sigma_{33}^2}\right)\\
R_{uv} &= \text{sign}(\langle uv\rangle)\left(a_{12}^2\sqrt{\frac{\pi}{2}}\sigma_{12}\right)\exp\left(-\frac{r^2}{2\sigma_{12}^2}\right)\\
R_{uw} &= \text{sign}(\langle uw\rangle)\left(a_{13}^2\sqrt{\frac{\pi}{2}}\sigma_{13}\right)\exp\left(-\frac{r^2}{2\sigma_{13}^2}\right)\\
R_{vw} &= \text{sign}(\langle vw\rangle)\left(a_{23}^2\sqrt{\frac{\pi}{2}}\sigma_{23}\right)\exp\left(-\frac{r^2}{2\sigma_{23}^2}\right)
\end{aligned}
\tag{11}
$$

Reynolds stresses for the generated velocity field can be easily obtained by setting $r=0$ in the expression for the correlation functions:

$$
\begin{aligned}
\langle uu\rangle &= \left(\sqrt{\frac{\pi}{2}}\right)[(a_{11}^2\sigma_{11})+(a_{12}^2\sigma_{12})+(a_{13}^2\sigma_{13})]\\
\langle vv\rangle &= \left(\sqrt{\frac{\pi}{2}}\right)[(a_{12}^2\sigma_{12})+(a_{22}^2\sigma_{22})+(a_{23}^2\sigma_{23})]\\
\langle ww\rangle &= \left(\sqrt{\frac{\pi}{2}}\right)[(a_{13}^2\sigma_{13})+(a_{23}^2\sigma_{23})+(a_{33}^2\sigma_{33})]\\
\langle uv\rangle &= \left(\sqrt{\frac{\pi}{2}}\right)(a_{12}^2\sigma_{12}).\text{sign}(\langle uv\rangle)\\
\langle uw\rangle &= \left(\sqrt{\frac{\pi}{2}}\right)(a_{13}^2\sigma_{13}).\text{sign}(\langle uw\rangle)\\
\langle vw\rangle &= \left(\sqrt{\frac{\pi}{2}}\right)(a_{23}^2\sigma_{23}).\text{sign}(\langle vw\rangle)
\end{aligned}
\tag{12}
$$

DOI: 10.1002/fld

Moreover, integral length scales can be analytically obtained based on Equation (2) (see Appendix C for more details):

$$
\begin{aligned}
l_{uu} &= \left(\frac{\pi}{2}\right)\frac{(a_{11}\sigma_{11})^2+(a_{12}\sigma_{12})^2+(a_{13}\sigma_{13})^2}{\langle uu\rangle}\\
l_{uu} &= \left(\frac{\pi}{2}\right)\frac{(a_{11}\sigma_{11})^2+(a_{12}\sigma_{12})^2+(a_{13}\sigma_{13})^2}{\langle uu\rangle}\\
l_{vv} &= \left(\frac{\pi}{2}\right)\frac{(a_{12}\sigma_{12})^2+(a_{22}\sigma_{22})^2+(a_{23}\sigma_{23})^2}{\langle vv\rangle}\\
l_{ww} &= \left(\frac{\pi}{2}\right)\frac{(a_{13}\sigma_{13})^2+(a_{23}\sigma_{23})^2+(a_{33}\sigma_{33})^2}{\langle ww\rangle}\\
l_{uv} &= \left(\sqrt{\frac{\pi}{2}}\right)\sigma_{12}\\
l_{uw} &= \left(\sqrt{\frac{\pi}{2}}\right)\sigma_{13}\\
l_{vw} &= \left(\sqrt{\frac{\pi}{2}}\right)\sigma_{23}
\end{aligned}
\tag{13}
$$

The set of Equations (12) and (13) express the 12 unknown coefficients of the method based on the 12 known statistical quantities, i.e. Reynolds-stresses and integral length scales. These sets of algebraic equations can be analytically solved to obtain the unknowns:

$$\sigma_{12}=\left(\sqrt{\frac{2}{\pi}}\right)l_{uv},\quad a_{12}=\sqrt{\frac{|\langle uv\rangle|}{l_{uv}}} \tag{14}$$

$$\sigma_{13}=\left(\sqrt{\frac{2}{\pi}}\right)l_{uw},\quad a_{13}=\sqrt{\frac{|\langle uw\rangle|}{l_{uw}}} \tag{15}$$

$$\sigma_{23}=\left(\sqrt{\frac{2}{\pi}}\right)l_{vw},\quad a_{23}=\sqrt{\frac{|\langle vw\rangle|}{l_{vw}}} \tag{16}$$

$$\sigma_{11}=\left(\sqrt{\frac{2}{\pi}}\right)\frac{(l_{uu})\langle uu\rangle-(l_{uv})|\langle uv\rangle|-(l_{uw})|\langle uw\rangle|}{\langle uu\rangle-|\langle uv\rangle|-|\langle uw\rangle|} \tag{17}$$

$$\sigma_{22}=\left(\sqrt{\frac{2}{\pi}}\right)\frac{(l_{vv})\langle vv\rangle-(l_{uv})|\langle uv\rangle|-(l_{vw})|\langle vw\rangle|}{\langle vv\rangle-|\langle uv\rangle|-|\langle vw\rangle|} \tag{18}$$

$$\sigma_{33}=\left(\sqrt{\frac{2}{\pi}}\right)\frac{(l_{ww})\langle ww\rangle-(l_{uw})|\langle uw\rangle|-(l_{vw})|\langle vw\rangle|}{\langle ww\rangle-|\langle vw\rangle|-|\langle uw\rangle|} \tag{19}$$

DOI: 10.1002/fld

$$a_{11} = \frac{\langle uu \rangle - |\langle uv \rangle| - |\langle uw \rangle|}{\sqrt{(l_{uu})\langle uu \rangle - (l_{uv})|\langle uv \rangle| - (l_{uw})|\langle uw \rangle|}} \tag{20}$$

$$a_{22} = \frac{\langle vv \rangle - |\langle uv \rangle| - |\langle vw \rangle|}{\sqrt{(l_{vv})\langle vv \rangle - (l_{uv})|\langle uv \rangle| - (l_{vw})|\langle vw \rangle|}} \tag{21}$$

$$a_{33} = \frac{\langle ww \rangle - |\langle uw \rangle| - |\langle vw \rangle|}{\sqrt{(l_{ww})\langle ww \rangle - (l_{uw})|\langle uw \rangle| - (l_{vw})|\langle vw \rangle|}} \tag{22}$$

With the filter widths and coefficients expressed in Equations (14)–(22), the velocity field can be generated based on Equations (10). Finally, this generated turbulent field u, v and w can be alternatively used as initial or inflow boundary condition. In the second application, a large volume of data can be generated, stored and subsequently convected through the inflow plane based on Taylor's hypothesis. However, the length of the stored data for inflow application should be long enough to avoid the introduction of flow periodicity through the domain.

3. APPLICATION OF THE NEW APPROACH

In this section, the proposed method is examined by generating turbulent initial conditions for homogeneous turbulent shear flow. To this end, different simulations, starting from various turbulent initial conditions, are compared with a reference simulation. These various turbulent initial conditions are generated, using extracted statistical information at a well-developed stage of the reference flow field in the self-similar period.

An overview of the main properties of different initial conditions used to initialize the simulations is given in Table I. The simplest initial condition, i.e. IC1, consists of white noise with prescribed turbulent kinetic energy components $\langle uu \rangle$, $\langle vv \rangle$ and $\langle ww \rangle$. Initial condition IC2 has complete Reynolds stresses information generated based on Lund's transformation [12]. Initial condition IC3 has prescribed turbulent kinetic energy components $\langle uu \rangle$, $\langle vv \rangle$, $\langle ww \rangle$ and normal integral length scales l_{uu}, l_{vv} and l_{ww}, generated by applying appropriate gaussian filters on the velocity field of IC1. Finally, initial condition IC4 is generated based on the new approach and satisfies both Reynolds stresses and integral length scales, l_{ij}, including cross-terms.

3.1. Reference homogeneous shear flow simulation

Homogeneous shear flow, where all the turbulent statistics are spatially uniform, can be considered as a bridge between the strongly idealized homogeneous isotropic turbulent flow and more realistic

Table I. Properties of different turbulent initial conditions used for different simulations. The imposed statistical quantities for each initial turbulent field are marked.

Initial conditions	$\langle u_i u_j \rangle$ where $i = j$	$\langle u_i u_j \rangle$ where $i \neq j$	l_{ij} where $i = j$	l_{ij} where $i \neq j$
IC1	✔	—	—	—
IC2	✔	✔	—	—
IC3	✔	—	✔	—
IC4	✔	✔	✔	✔

DOI: 10.1002/fld

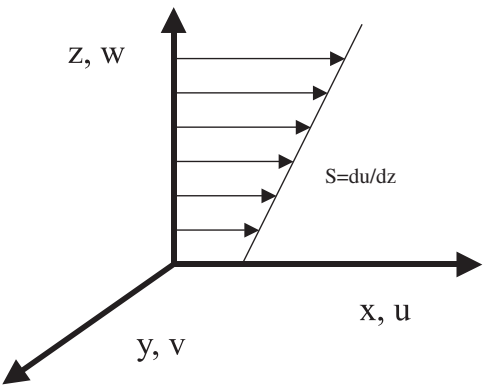

Figure 2. A sketch of the mean velocity profile in homogeneous shear flow and coordinate system.

turbulent shear flows such as mixing layer and plane jet. This test case has been mainly investigated to examine the effects of anisotropy of large scales, to examine the existence of the organized structures in turbulence and to develop models for inhomogeneous turbulent flows [30–33].

Apart from simple geometry and boundary conditions, other characteristics of this flow make it an appropriate test case for this research. First, this test case is a temporally evolving shear flow showing a self-similar state. That is, when statistics are normalized by appropriate quantities, they become independent of time [34–36]. Therefore, the impact of different initial conditions on the asymptotic flow-field behavior—which can be interpreted as the effect of different upstream boundary conditions on the stationary state for a spatially evolving turbulent flow—can be investigated with an affordable computational cost. Secondly, the effects of the cross-integral length scales on the flow-field behavior can be better appreciated due to the existence of anisotropic large-scale structures in this flow field. Finally, flow-field homogeneity and spanwise symmetry reduce the required statistical information for the above-mentioned initial conditions. It can be shown that the spanwise velocity component v is uncorrelated with streamwise and normal components u and w. Therefore, their respective Reynolds stresses $\langle uv\rangle$, $\langle vw\rangle$ and integral length scales l_{uv}, l_{vw} are zero.

In the considered temporal homogeneous turbulent shear flow, the imposed mean flow in streamwise direction x is a linear function of the normal coordinate z:

$$U(z) = Sz \tag{23}$$

where S is the mean shear rate (see Figure 2). The homogeneous shear flow results presented in this paper are taken from low and high shear rate simulations. For all simulations kinematic viscosity is $v = 0.001$. For low shear rate simulations $S = 10.0$ and for high shear rate simulations $S = 20.0$, where all the flow-field parameters are in arbitrary units. The fully compressible NS equations are solved, for the fluctuating part of the velocity field $\mathbf{u}(\mathbf{x}, t)$, only [37]

$$\mathbf{U}(\mathbf{x}, t) = U(z)\mathbf{e_x} + \mathbf{u}(\mathbf{x}, t) \tag{24}$$

where $\mathbf{U}(\mathbf{x}, t)$ is the complete velocity field and $\mathbf{e_x}$ is the unit vector in streamwise direction x. The set of NS equations are solved based on a cell-averaged finite-volume approach. Convective and viscous fluxes are discretized on a uniform mesh with 100^3 grid cells, with grid spacing

DOI: 10.1002/fld

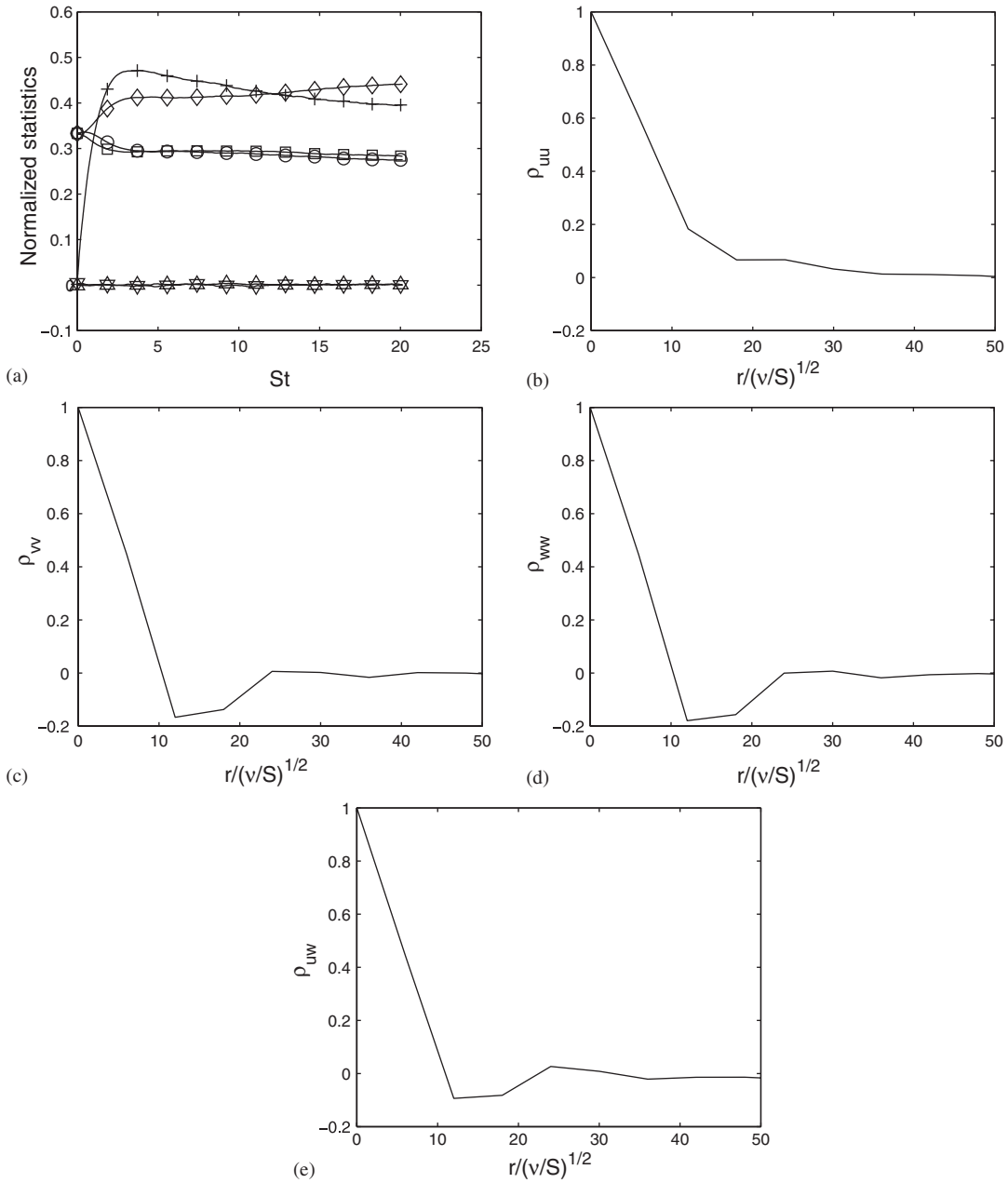

Figure 3. History of Reynolds stress components evolution and correlation coefficients of reference homogeneous turbulent shear flow simulation. (a) The normalized Reynolds stresses: (—◇—), $\langle uu\rangle/q$; (—○—), $\langle vv\rangle/q$; (—□—), $\langle ww\rangle/q$; (—+—), $-\langle uw\rangle/(u'w')$; (—△—), $\langle uv\rangle/(u'v')$; (—▽—), $\langle vw\rangle/(v'w')$, where $q=\langle u_i u_i\rangle$, $u'=\sqrt{\langle uu\rangle}$, $v'=\sqrt{\langle vv\rangle}$ and $w'=\sqrt{\langle ww\rangle}$; (b)–(e) correlation coefficients ρ_{uu}, ρ_{vv}, ρ_{ww} and ρ_{uw} at $St^*=5.88$.

DOI: 10.1002/fld

Table II. Flow-field statistic for the low shear rate reference simulation at $St^*=5.88$; $q=\langle u_i u_i\rangle$ with summation convention, $u'=\sqrt{\langle uu\rangle}$ and $w'=\sqrt{\langle ww\rangle}$.

$\frac{\langle uu\rangle_{\text{ref}}}{q}$	$\frac{\langle vv\rangle_{\text{ref}}}{q}$	$\frac{\langle ww\rangle_{\text{ref}}}{q}$	$\frac{\langle uw\rangle_{\text{ref}}}{u'w'}$	$\frac{l_{uu}^{\text{ref}}}{(\nu/S)^{1/2}}$	$\frac{l_{vv}^{\text{ref}}}{(\nu/S)^{1/2}}$	$\frac{l_{ww}^{\text{ref}}}{(\nu/S)^{1/2}}$	$\frac{l_{uw}^{\text{ref}}}{(\nu/S)^{1/2}}$
0.4114	0.2933	0.2953	−0.4581	18.6338	16.2465	16.7035	16.0960

$\Delta x/(\nu/S)^{1/2}$ equal to 6 and 3, respectively, for low and high shear rate simulations, using a second-order discretization. For time integration an explicit four-stage compact-storage Runge–Kutta scheme of second-order accuracy with coefficients $[\frac{1}{4}, \frac{1}{3}, \frac{1}{2}, 1]$ is used. Since no subgrid scale model has been introduced to the set of equations, simulations can be considered as a coarse DNS based on this grid spacing. Although using high-order discretizations or spectral methods is more usual for solving this test case due to its simple geometry, in this research a second-order scheme is considered as will be explained. Besides very successful DNS computations using second-order schemes (see [38, 39]), most of the LES computations are performed based on the low-order discretization methods. Therefore, using this low-order DNS computation can also reveal the performance of this stochastic method in LES simulations without influencing the results by subgrid scale model effects.

Figure 3 shows the flow-field correlation functions at a specific non-dimensional time $St^*=St^*=5.88$ and the evolution of the Reynolds stress components for the low shear rate reference simulation. This reference simulation is started from an isotropic turbulent velocity field with top hat energy spectrum over wave numbers $16<k<32$ [40]. From Figure 3(a) it can be clearly observed that the normalized Reynolds stresses almost achieve a constant level after non-dimensional time $St\approx 4$ which indicates that the flow field is in a self-similar state. Also it can be seen that $\langle uv\rangle$ and $\langle vw\rangle$ remain zero during the flow-field evolution which reflects the spanwise symmetry property of the homogeneous turbulent shear flow. This also reveals that this computational resolution provides enough spatial ensembles to capture the main averaged properties of the homogeneous turbulent shear flow.

The flow field at $St^*=5.88$ is saved and the required statistical quantities are extracted and presented in Table II. However, with respect to the computed statistical quantities in Table II, two issues have to be emphasized on. First issue is related to the correlation coefficient ρ_{ij} with negative region or negative overshoot in Figure 3(c)–(e). As already mentioned in Section 2.1, in the proposed method the random flow field is generated using a spherically symmetric gaussian filter function. Consequently, the established correlation shows an approximately gaussian shape which is a positive-definite function and cannot represent negative overshoot. This problem is dealt with by computing integral length scales based on the absolute value of the correlation function [3],

$$l_{ij}(\mathbf{x})=\int_0^\infty |\rho_{ij}(\mathbf{x}, r\mathbf{e})|\,\mathrm{d}r \tag{25}$$

Second issue is related to the different values of the integral length scales in different directions. Because of the spherical symmetry of the filter function, the proposed method is able to generate velocity field with unique integral length scale for each velocity component in all directions. This restriction is solved by considering the largest integral length scale for each velocity component which for this test case is in streamwise direction, i.e. the integral length scales in Equation (25) are computed based on the separation direction $r\mathbf{e}_\mathbf{x}$.

DOI: 10.1002/fld

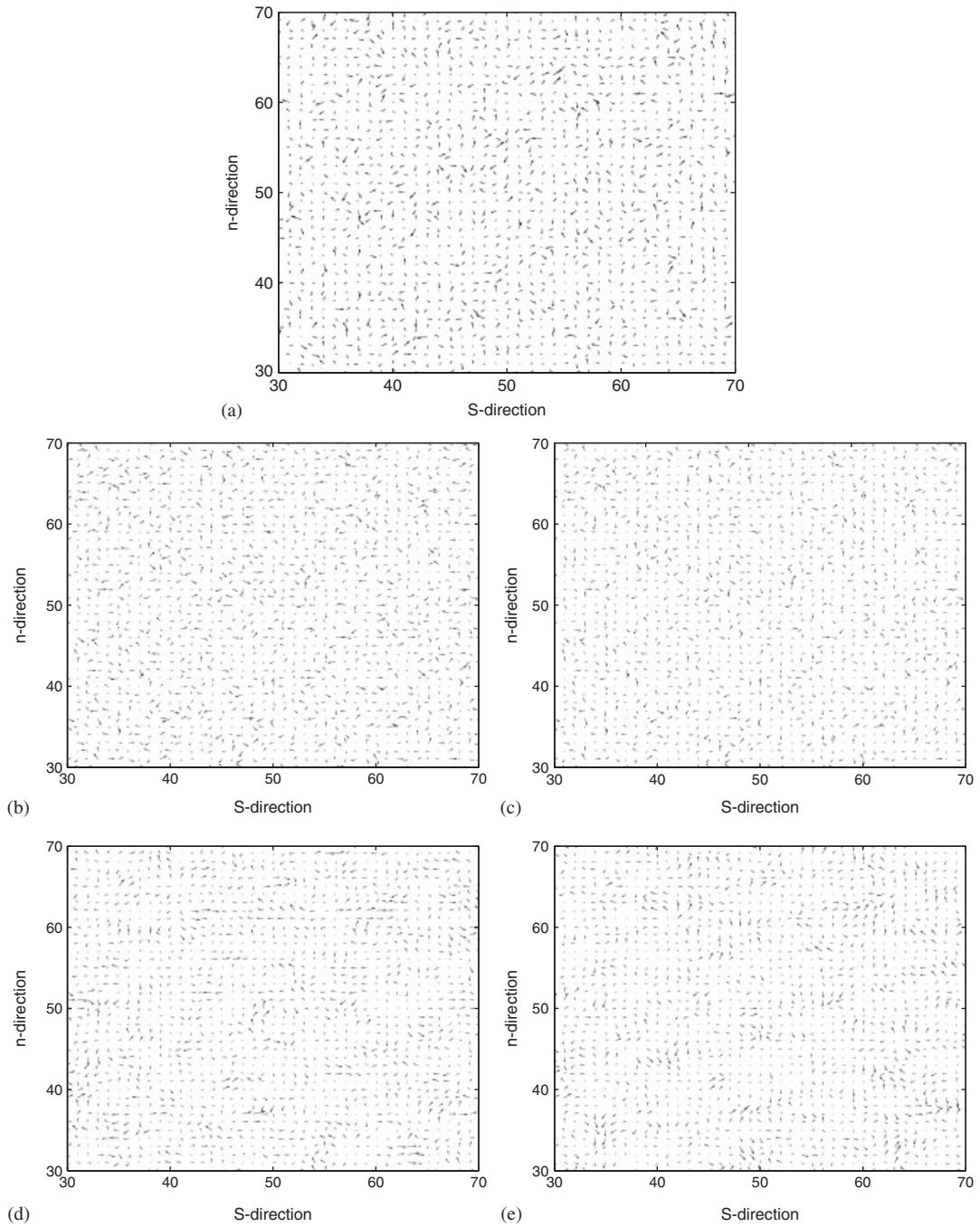

Figure 4. Projection of the instantaneous initial vorticity vectors on a plane inclined at 45°; s-direction is along and n-direction is normal to the plane. (a) Reference vorticity field at $St = St^*$; (b) IC1; (c) IC2; (d) IC3; and (e) IC4.

DOI: 10.1002/fld

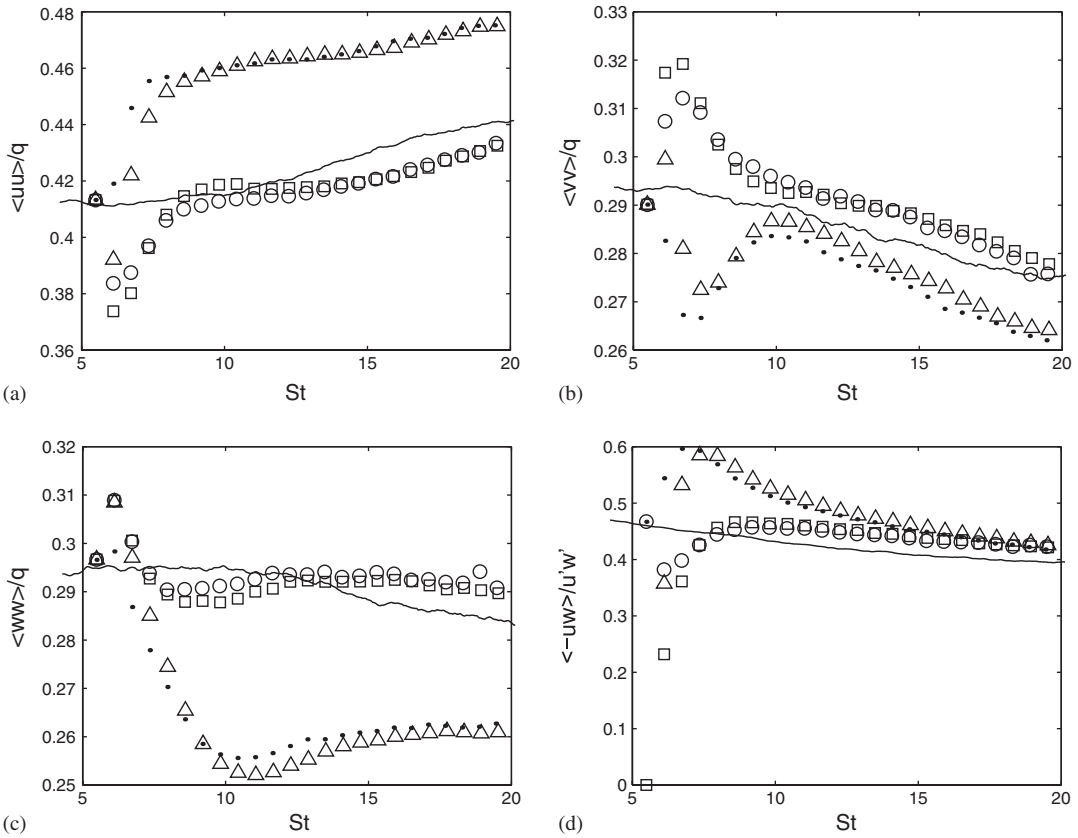

Figure 5. Flow-field evolution of homogeneous turbulent shear flow, initialized with different random fields: (a) $\langle uu\rangle/q$; (b) $\langle vv\rangle/q$; (c) $\langle ww\rangle/q$; and (d) $-\langle uw\rangle/u'w'$, where $q=\langle u_i u_i\rangle$, $u'=\sqrt{\langle uu\rangle}$ and $w'=\sqrt{\langle ww\rangle}$; (—), reference simulation (low shear rate); (○), IC4 or new approach (all the Reynolds stress and integral length scales imposed); (□), IC3 (only normal Reynolds stresses and integral length scales imposed); (.), IC2 (all the Reynolds stress components imposed); (△), IC1 (only normal Reynolds stress components imposed).

The presented quantities in Table II, computed based on the above-mentioned issues, are subsequently used to generate different random turbulent initial conditions.

3.2. Comparison of different initial conditions

In this section, to examine the capability of the method, several simulations are carried out for a homogeneous turbulent shear flow, starting at $St=St^*$. Turbulent velocity fields for these simulations are initialized by different turbulent velocity fields, satisfying different level of target statistics, corresponding to IC1, IC2, IC3 and IC4, elaborated in Table I.

First, to provide a direct way to qualitatively compare different initial conditions, the instantaneous flow-field CS are demonstrated using instantaneous vorticity field. Figure 4 shows the projection of the instantaneous initial vorticity vectors on a plane inclined at 45° (the direction of principal elongation of the mean strain). On the basis of the previous observations [31], it is

DOI: 10.1002/fld

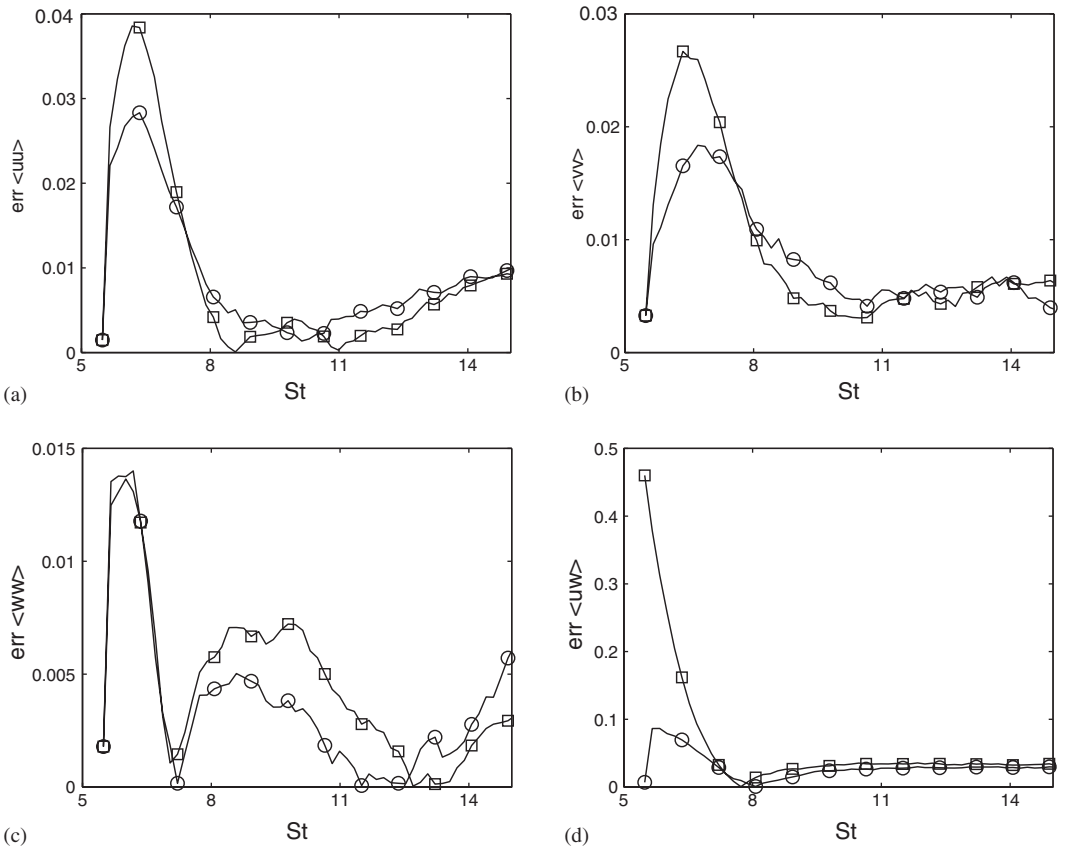

Figure 6. Evolution of the deviation of the Reynolds stress components from low shear rate reference simulation: (a) $\langle uu \rangle$; (b) $\langle vv \rangle$; (c) $\langle ww \rangle$; and (d) $\langle uw \rangle$ where deviations are computed based on Equation (27). (—○—), IC4 or new approach, for which all the Reynolds stress and integral length scale components are imposed; (—□—), IC3, for which only normal Reynolds stress and integral length scale components are imposed.

known that vortex tubes, are mainly inclined at 45° to the flow direction. It can be observed that initial conditions, IC3 and IC4, are more capable to produce CS.

Figure 5 shows the evolution of the normalized Reynolds stress components for these simulations. Comparing the evolution of these quantities in Figure 5 reveals that the flow field started from initial condition with prescribed integral length scales, i.e. IC4 and IC3 are much closer to the low shear rate reference simulation. Moreover, using initial velocity field IC4, generated based on the new procedure, results in more accurate flow-field evolution compared with the simulation with only prescribed normal integral length scale IC3. The difference between these two cases can be better observed by considering their total deviation from the reference simulation as a measure for the total integral error,

$$\mathrm{err}_{\mathrm{tot}}(\phi) = \int_{\tau=St^*}^{\tau=20} \mathrm{err}_{\phi}(\tau)\,\mathrm{d}\tau \tag{26}$$

DOI: 10.1002/fld

Table III. Total deviation for all simulations for low shear rate simulations; $q=\langle u_i u_i\rangle$, $u'=\sqrt{\langle uu\rangle}$, $w'=\sqrt{\langle ww\rangle}$. $\langle uu\rangle/q_{\mathrm{IC4}}=0.1311$, $\langle vv\rangle/q_{\mathrm{IC4}}=0.0946$, $\langle ww\rangle/q_{\mathrm{IC4}}=0.0639$, $\langle uw\rangle/u'w'_{\mathrm{IC4}}=0.4093$.

	IC4	IC3	IC2	IC1
Total error for $\frac{\langle uu\rangle}{q}/\frac{\langle uu\rangle}{q}_{\mathrm{IC4}}$	1.0000	1.0117	3.9239	3.7668
Total error for $\frac{\langle vv\rangle}{q}/\frac{\langle vv\rangle}{q}_{\mathrm{IC4}}$	1.0000	1.1496	1.5848	1.1524
Total error for $\frac{\langle ww\rangle}{q}/\frac{\langle ww\rangle}{q}_{\mathrm{IC4}}$	1.0000	1.0383	5.7538	6.0832
Total error for $\frac{\langle uw\rangle}{u'w'}/\frac{\langle uw\rangle}{u'w'}_{\mathrm{IC4}}$	1.0000	1.6597	2.1895	2.6312

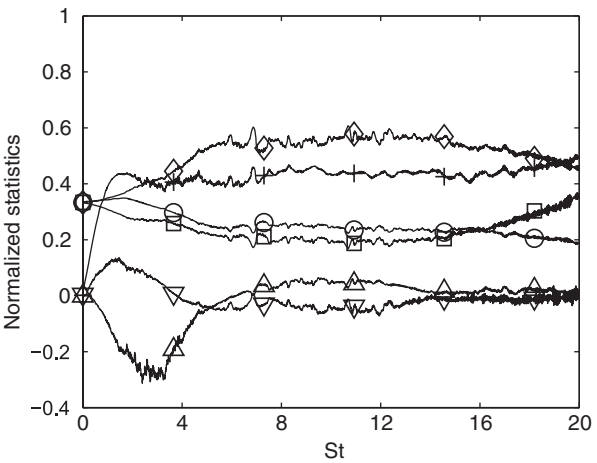

Figure 7. History of the normalized Reynolds stress components evolution for the homogeneous shear flow with high shear rate $S=20$; (—◇—), $\langle uu\rangle/q$; (—○—), $\langle vv\rangle/q$; (—□—), $\langle ww\rangle/q$; (—+—), $-\langle uw\rangle/(u'w')$; (—△—), $\langle uv\rangle/(u'v')$; (—∇—), $\langle vw\rangle/(v'w')$, where $q=\langle u_i u_i\rangle$, $u'=\sqrt{\langle uu\rangle}$, $v'=\sqrt{\langle vv\rangle}$ and $w'=\sqrt{\langle ww\rangle}$.

where

$$\mathrm{err}_\phi(\tau)=\sqrt{(\overline{\phi}(\tau)-\overline{\phi}_{\mathrm{ref}}(\tau))^2} \tag{27}$$

and $\overline{\phi}$ represents the normalized Reynolds stress components.

Figure 6 shows this error for two simulations initialized by IC4 and IC3. Although both simulations are close to each other, it can be observed that data generated from the new procedure show smaller deviation from the reference simulation, especially in the initial phase of the simulation. Computing total deviations from the reference simulation during computation time confirms that the most accurate results are obtained from initial condition where all the Reynolds stresses and integral length scales are prescribed, i.e. IC4. Listed in Table III are total errors for all simulations computed based on Equation (26) and normalized with the total error of IC4.

DOI: 10.1002/fld

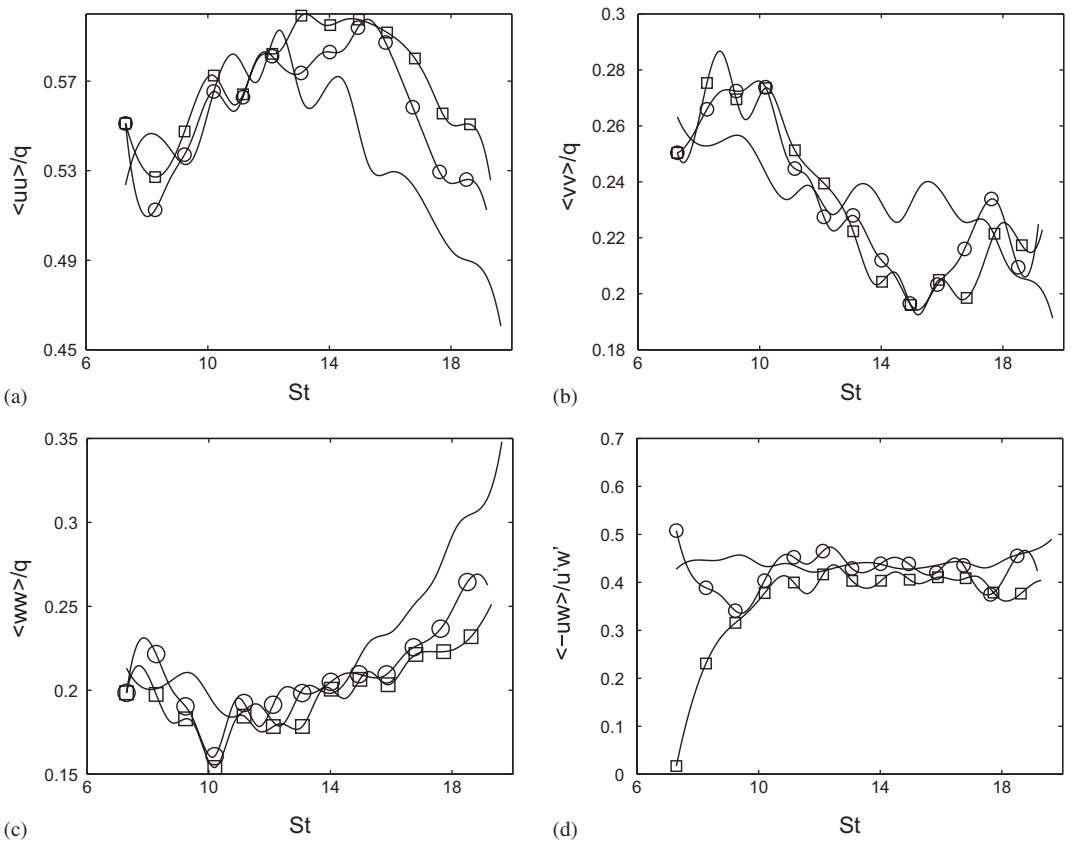

Figure 8. Flow-field evolution of homogeneous turbulent shear flow with higher shear rate $S=20$, initialized with random fields IC3 and IC4. (a) $\langle uu\rangle/q$; (b) $\langle vv\rangle/q$; (c) $\langle ww\rangle/q$; and (d) $-\langle uw\rangle/u'w'$, where $q=\langle u_i u_i\rangle$, $u'=\sqrt{\langle uu\rangle}$ and $w'=\sqrt{\langle ww\rangle}$. (—), reference simulation; (○), IC4 or new approach, for which all the Reynolds stress and integral length scale components are imposed; (□), IC3, for which only normal Reynolds stress and integral length scale components are imposed.

For flow fields with high level of anisotropy, it is expected that the effects of the anisotropic parts of the correlation function and consequently related statistical quantities such as cross-integral length scales become more important. To examine the influence of higher anisotropy, the higher shear rate reference simulation is considered with the same resolution, initial condition and kinematic viscosity explained in Section 3.1 while the shear rate is doubled, i.e. $S=20$.

Figure 7 shows the evolution of the Reynolds stress components for high-shear rate simulation. The oscillations of the Reynolds stress components and non-zero values of $\langle uv\rangle$ and $\langle vw\rangle$ (specifically before $St\sim 6$) show that the used resolution is too coarse to provide enough ensembles. However, after a transient period the solution shows a plateau region. At non-dimensional time $St=7.3$, the required statistical information is extracted from the flow field to generate two turbulent velocity fields based on IC3 and IC4 which are used for simulations.

DOI: 10.1002/fld

Table IV. Total deviation from high shear flow-field reference for simulations initialized with IC3 and IC4; $q=\langle u_i u_i\rangle$, $u'=\sqrt{\langle uu\rangle}$, $w'=\sqrt{\langle ww\rangle}$. $\langle uu\rangle/q_{\mathrm{IC4}}=0.3581$, $\langle vv\rangle/q_{\mathrm{IC4}}=0.2371$, $\langle ww\rangle/q_{\mathrm{IC4}}=0.2729$, $\langle uw\rangle/u'w'_{\mathrm{IC4}}=0.49$.

	IC4	IC3
Total error for $\frac{\langle uu\rangle}{q}/\frac{\langle uu\rangle}{q}_{\mathrm{IC4}}$	1.0000	1.3675
Total error for $\frac{\langle vv\rangle}{q}/\frac{\langle vv\rangle}{q}_{\mathrm{IC4}}$	1.0000	1.1783
Total error for $\frac{\langle ww\rangle}{q}/\frac{\langle ww\rangle}{q}_{\mathrm{IC4}}$	1.0000	1.4357
Total error for $\frac{\langle uw\rangle}{u'w'}/\frac{\langle uw\rangle}{u'w'}_{\mathrm{IC4}}$	1.0000	1.9330

Figure 8 shows the evolution of the normalized Reynolds stress components for these simulations. To remove the wiggles, figures are smoothed out with interpolation. Although both solutions closely follow the reference simulation, the total errors presented in Table IV reveal that the new procedure results in more accurate simulation. Moreover, by comparing the errors between IC4 and IC3 in Tables III and IV it can be observed that increasing the shear rate also increases deviation between simulations started from IC4 and IC3.

To recapitulate, simulations initialized by the new procedure where all the Reynolds stress components and integral length scales are prescribed show a more accurate flow-field evolution compared with simulations initialized with initial conditions containing less statistical information. Comparing the low and high shear rate cases, it is clear that the impact of considering cross-integral length scales in the generation procedure becomes more important at higher level of anisotropy.

4. CONCLUSION

A new stochastic method for generating an artificial turbulent velocity field for DNS and LES has been developed and tested. This method generates a fluctuating velocity field that satisfies both prescribed local integral length scales, including cross-integral length scales and Reynolds stresses. In this method, first by filtering individual random white-noise fields, different uncorrelated random fields with prespecified gaussian autocorrelation functions are generated. Subsequently, these random fields are combined with appropriate coefficients to generate the final turbulent velocity field. The application of the proposed method is inexpensive and does not require periodic directions.

To examine the application of the proposed method, different numerical simulations of a temporally developing homogeneous turbulent shear flow have been performed. Turbulent velocity fields are used to initialize the simulations containing different levels of statistical information. Comparing the simulation results with a reference simulation revealed that the new procedure yields velocity field with more complete spectral content and consequently more accurate results. Moreover, by increasing the shear rate, the impact of the considered cross-integral length scale information in the initial condition on the flow-field evolution becomes more important.

DOI: 10.1002/fld

APPENDIX A: CORRELATION OF A RANDOM VELOCITY FIELD

In this Appendix, it is shown that the correlation functions of the velocity field described by Equation (3) can be expressed by Equation (4). For convenience, only u and R_{uu} are considered. Let f_{11}, f_{12} and f_{13} be three random uncorrelated fields, i.e.

$$\mathrm{corr}(f_{ij} f_{mn}) = \langle f_{ij} f_{mn} \rangle = \delta_{im} \delta_{jn} \tag{A1}$$

where $\mathrm{corr}(f, h)$ means correlation function for two signals $f(x)$ and $h(x)$:

$$\mathrm{corr}(f, h) = \int_{-\infty}^{+\infty} f(x) h(x+r)\, \mathrm{d}x \tag{A2}$$

Furthermore, the Fourier transform of function $f(x)$, $\widehat{f}$ is denoted by

$$\widehat{f}(k) = \mathscr{F}\mathscr{T}(f) = \int_{-\infty}^{+\infty} f(x) \exp(-2\pi \mathrm{i} k x)\, \mathrm{d}x \tag{A3}$$

Using the following Fourier transform pairs:

$$af + bh \iff a\widehat{f} + b\widehat{h} \tag{A4}$$

$$\mathrm{corr}(f, h) \iff \widehat{f}.\widehat{h}^* \tag{A5}$$

where * in Fourier transformation means conjugate. It can be seen for velocity component $u = a_{11} f_{11} + a_{12} f_{12} + a_{13} f_{13}$, the autocorrelation R_{uu} is

$$\begin{aligned} R_{uu} &= \mathscr{F}\mathscr{T}^{-1}\{\widehat{u}.\widehat{u}^*\} \\ &\overset{(A4),(A5)}{=} \mathscr{F}\mathscr{T}^{-1}\{(a_{11}\widehat{f}_{11} + a_{12}\widehat{f}_{12} + a_{13}\widehat{f}_{13}).(a_{11}\widehat{f}^*_{11} + a_{12}\widehat{f}^*_{12} + a_{13}\widehat{f}^*_{13})\} \\ &\overset{(A1)}{=} \mathscr{F}\mathscr{T}^{-1}\{a_{11}^2 \widehat{f}_{11}\widehat{f}^*_{11} + a_{12}^2 \widehat{f}_{12}\widehat{f}^*_{12} + a_{13}^2 \widehat{f}_{13}\widehat{f}^*_{13}\} \\ R_{uu} &= \{a_{11}^2 r_{11} + a_{12}^2 r_{12} + a_{13}^2 r_{13}\} \end{aligned} \tag{A6}$$

APPENDIX B: CORRELATION FOR GENERATED VELOCITY FIELD BASED ON THE PROPOSED METHOD

In this Appendix, it is shown that the correlation functions of the velocity field described by Equation (10) can be expressed by Equation (11). For convenience, only u and R_{uu} are considered. Velocity component u is

$$u = a_{11} \exp\left(-\frac{r^2}{\sigma_{11}^2}\right) \circ \xi_{11} + a_{12} \exp\left(-\frac{r^2}{\sigma_{12}^2}\right) \circ \xi_{12} + a_{13} \exp\left(-\frac{r^2}{\sigma_{13}^2}\right) \circ \xi_{13}$$

DOI: 10.1002/fld

where ξ_{ij} are uncorrelated white noises satisfying Equation (7), σ_{ij} are filter widths, a_{ij} are coefficients and $\circ$ denotes filtering. Using the following Fourier transform pairs:

$$\exp\left(-\frac{x^2}{a^2}\right) \iff \sqrt{\pi}a\exp(-\pi^2k^2a^2) \tag{B1}$$

$$(f\circ h) \iff \widehat{f}.\widehat{h} \tag{B2}$$

where $(f\circ h)$ means filtering or convolution:

$$(f\circ h)=\int_{-\infty}^{+\infty} f(x)h(x-r)\,\mathrm{d}x \tag{B3}$$

The correlation function for velocity component u can be written as

$$R_{uu}=\mathscr{F}\mathscr{T}^{-1}\{\widehat{u}.\widehat{u}^*\}$$

where the Fourier transformation of u equals

$$\begin{aligned}\widehat{u}\overset{(B1),(B2)}{=}\ &(\sqrt{\pi}a_{11}\sigma_{11})\exp(-\pi^2k^2\sigma_{11}^2).\hat{\xi}_{11}+(\sqrt{\pi}a_{12}\sigma_{12})\exp(-\pi^2k^2\sigma_{12}^2).\hat{\xi}_{12}\\ &+(\sqrt{\pi}a_{13}\sigma_{11})\exp(-\pi^2k^2\sigma_{13}^2).\hat{\xi}_{13}\end{aligned} \tag{B4}$$

Therefore, R_{uu} is

$$\begin{aligned}R_{uu}\overset{(A5),(A7)}{=}\ &\mathscr{F}\mathscr{T}^{-1}\{(\sqrt{\pi}a_{11}\sigma_{11})^2\exp(-2\pi^2k^2\sigma_{11}^2).(\hat{\xi}_{11}\hat{\xi}_{11}^*)\}\\ &+\mathscr{F}\mathscr{T}^{-1}\{(\sqrt{\pi}a_{12}\sigma_{12})^2\exp(-2\pi^2k^2\sigma_{12}^2).(\hat{\xi}_{12}\hat{\xi}_{12}^*)\}\\ &+\mathscr{F}\mathscr{T}^{-1}\{(\sqrt{\pi}a_{13}\sigma_{13})^2\exp(-2\pi^2k^2\sigma_{13}^2).(\hat{\xi}_{13}\hat{\xi}_{13}^*)\}\end{aligned}$$

Applying the inverse Fourier transformation results in

$$\begin{aligned}R_{uu}=&\left(a_{11}^2\sqrt{\frac{\pi}{2}}\sigma_{11}\right)\exp\left(-\frac{r^2}{2\sigma_{11}^2}\right)+\left(a_{12}^2\sqrt{\frac{\pi}{2}}\sigma_{12}\right)\exp\left(-\frac{r^2}{2\sigma_{12}^2}\right)\\ &+\left(a_{13}^2\sqrt{\frac{\pi}{2}}\sigma_{13}\right)\exp\left(-\frac{r^2}{2\sigma_{13}^2}\right)\end{aligned} \tag{B5}$$

APPENDIX C: INTEGRAL LENGTH SCALE FOR GENERATED VELOCITY FIELD

In this Appendix, it is shown that the integral length scales for the velocity field described by Equation (10) can be expressed by Equation (13). Integral length scales are related to the normalized correlation function. In this research, for simplicity, the correlation functions are normalized with their particular Reynolds stresses:

$$l_{ij}(\mathbf{x})=\int_0^\infty \frac{R_{ij}(\mathbf{x},r\mathbf{e}_1)}{R_{ij}(\mathbf{x},0)}\,\mathrm{d}r=\frac{1}{\langle u_iu_j\rangle}\int_0^\infty R_{ij}(\mathbf{x},r\mathbf{e}_1)\,\mathrm{d}r \tag{C1}$$

DOI: 10.1002/fld

where $\mathbf{e}_1$ is the unit vector in one of the x, y or z direction. However, in this method the applied filter function is an isotropic Gaussian function which produces correlation function with spherical symmetry. Therefore, established integral length scales are also isotropic

$$l_{ij}(\mathbf{x}) = \frac{1}{\langle u_i u_j \rangle} \int_0^\infty R_{ij}(\mathbf{x}; r\mathbf{e}_x, 0, 0)\,\mathrm{d}r = \frac{1}{\langle u_i u_j \rangle} \int_0^\infty R_{ij}(\mathbf{x}; 0, r\mathbf{e}_y, 0)\,\mathrm{d}r$$
$$= \frac{1}{\langle u_i u_j \rangle} \int_0^\infty R_{ij}(\mathbf{x}; 0, 0, r\mathbf{e}_z)\,\mathrm{d}r \tag{C2}$$

Integral length scales can be related to the velocity spectrum tensor ϕ_{ij}, i.e. the Fourier transform of the two-point correlation function

$$\Phi_{ij}(\kappa) = \int_{-\infty}^{+\infty} \mathrm{e}^{-\mathrm{i}\kappa.\mathbf{r}} R_{ij}(\mathbf{r})\,\mathrm{d}\mathbf{r} = 2\int_0^{+\infty} \mathrm{e}^{-\mathrm{i}\kappa.\mathbf{r}} R_{ij}(\mathbf{r})\,\mathrm{d}\mathbf{r} \tag{C3}$$

Therefore, integral length scales can be easily extracted from Equation (C3) by setting $\kappa = 0$:

$$l_{ij} = \frac{1}{2\langle u_i u_j \rangle} \Phi_{ij}(0) \tag{C4}$$

Considering the fact that $\Phi_{ij}(\kappa) = \widehat{u}_i \widehat{u}_j^*$, where $\widehat{u}_i$ is the Fourier transform of u_i velocity component, integral length scale l_{ii} can be written as follows:

$$\Phi_{uu}(k) \overset{\text{(B4),(C3)}}{=} \{(\sqrt{\pi} a_{11}\sigma_{11})^2 \exp(-2\pi^2 k^2 \sigma_{11}^2).(\hat{\xi}_{11}\hat{\xi}_{11}^*)\}$$
$$+\{(\sqrt{\pi} a_{12}\sigma_{12})^2 \exp(-2\pi^2 k^2 \sigma_{12}^2).(\hat{\xi}_{12}\hat{\xi}_{12}^*)\}$$
$$+\{(\sqrt{\pi} a_{13}\sigma_{13})^2 \exp(-2\pi^2 k^2 \sigma_{13}^2).(\hat{\xi}_{13}\hat{\xi}_{13}^*)\}$$

considering orthogonality of random fields ξ_{ij} expressed by Equation (7)

$$\Phi_{uu}(k) \overset{(7)}{=} \{(\sqrt{\pi} a_{11}\sigma_{11})^2 \exp(-2\pi^2 k^2 \sigma_{11}^2)\} + \{(\sqrt{\pi} a_{12}\sigma_{12})^2 \exp(-2\pi^2 k^2 \sigma_{12}^2)\}$$
$$+\{(\sqrt{\pi} a_{13}\sigma_{13})^2 \exp(-2\pi^2 k^2 \sigma_{13}^2)\} \tag{C5}$$

Therefore, based on Equation (C4)

$$l_{uu} = \left(\frac{\pi}{2}\right) \frac{(a_{11}\sigma_{11})^2 + (a_{12}\sigma_{12})^2 + (a_{13}\sigma_{13})^2}{\langle uu \rangle} \tag{C6}$$

DOI: 10.1002/fld

NOMENCLATURE

$\mathbf{e}$	unit vector [L]
$\mathbf{x}$	spatial coordinate vector [L]
$\mathbf{r}$	spatial separation vector [L]
t	time [T]
ν	kinematic viscosity (μ/ρ) [LT^{-1}]
κ	wave number [L^{-1}]
$\Phi_{ij}(\kappa)$	velocity–spectrum tensor [L^3T^{-2}]
$R_{ij}(\mathbf{x},\mathbf{r})$	two-point velocity correlation [L^2T^{-2}]
$\rho_{ij}(\mathbf{x},\mathbf{r})$	two-point velocity correlation coefficient $\left(\frac{R_{ij}(\mathbf{x},\mathbf{r})}{R_{ij}(\mathbf{x},0)}\right)$
$\langle\rangle$	ensemble average
l_{ij}	integral length scale for velocity components i and j [L]
f_{ij}	random field with specific autocorrelation and zero mean
ξ_{ij}, ψ_{ij}	uncorrelated random field with zero mean
r_{ij}	autocorrelation function for random field f_{ij}
a_{ij}	coefficients
σ_{ij}	filter width [L]
F_{ij}	gaussian filter with filter width σ_{ij}
S	shear rate [T^{-1}]
St	non-dimensional time ($S.t$)
$\mathbf{U}(\mathbf{x},t)$	complete velocity field [LT^{-1}]
$\mathbf{u}(\mathbf{x},t)$	fluctuating part of velocity field [LT^{-1}]

Abbreviations

NS	Navier–Stokes
DNS	direct numerical simulation
RANS	Reynolds-averaged Navier–Stokes
CS	coherent structures

Subscripts

x	streamwise direction [L]
y	spanwise direction [L]
z	normal direction [L]

ACKNOWLEDGEMENTS

This research was performed in the framework of FWO-project G.0130.02. The authors are grateful for the financial support by FWO-Vlaanderen.

REFERENCES

1. Grinstein FF. Introduction: boundary conditions for large eddy simulation. *AIAA Journal* 2004; **42**(3):437.
2. George WK, Davidson L. Role of initial conditions in establishing asymptotic flow behavior. *AIAA Journal* 2004; **42**(3):438–447.

DOI: 10.1002/fld

3. Frisch U. *Turbulence*. Cambridge University Press: Cambridge, 1995.
4. Holmes P, Lumley JL, Berkooz G. *Turbulence*, *Coherent Structures*, *Dynamical Systems and Symmetry*. Cambridge University Press: Cambridge, 1996.
5. Hilborn RC. *Chaos and Nonlinear Dynamics*. Oxford University Press: Oxford, 1994.
6. Hussain AKMF, Zedan MF. Effects of the initial condition on the axi-symmetric free shear layer: effects of the initial momentum thickness. *Physics of Fluids* 1978; **21**(7):1100–1112.
7. Dziomba B, Fiedler HE. Effect of initial conditions on two-dimensional free shear layers. *Journal of Fluid Mechanics* 1985; **152**:419–442.
8. Bell JH. Development of a two-stream mixing layer from tripped and untripped boundary layer. *AIAA Journal* 1990; **28**:2034–2042.
9. Balaras E, Piomelli U, Wallace JM. Self-similar states in turbulent mixing layers. *Journal of Fluid Mechanics* 2001; **446**:1–24.
10. Moser RD, Rogers MM. The three-dimensional evolution of a plane mixing layer: pairing and transition to turbulence. *Journal of Fluid Mechanics* 1993; **247**:275–320.
11. Rogers MM, Moser RD. The three-dimensional evolution of a plane mixing layer: the Kelvin–Helmholtz rollup. *Journal of Fluid Mechanics* 1992; **243**:183–226.
12. Lund TS, Wu X, Squires KD. Generation of turbulent inflow data for spatially-developing boundary layer simulations. *Journal of Computational Physics* 1998; **140**:233–258.
13. Rogers MM, Moser RD. Direct simulation of a self similar turbulent mixing layer. *Physics of Fluids* 1994; **6**:903–923.
14. Li N, Balaras E, Piomelli U. Inflow conditions for large-eddy simulations of mixing layers. *Physics of Fluids* 2000; **12**(4):935.
15. Sagaut P. *Large Eddy Simulations for Incompressible Flows*, *Scientific Computation* (2nd edn). Springer: Berlin, 2002.
16. Monin AS, Yaglom AM. *Statistical Fluid Mechanics*: *Mechanics of Turbulence*, vol. 2. MIT Press: Cambridge, MA, 1975.
17. Lee S, Lele SK, Moin P. Simulation of spatially evolving turbulence and the applicability of Taylor's hypothesis in compressible flow. *Physics of Fluids A* 1992; **4**(7):1521–1530.
18. Kondo K, Mochida A, Murakami S. Generation of velocity fluctuations for inflow boundary conditions of LES. *Journal of Wind Engineering and Industrial Aerodynamics* 1997; **67–68**:51–64.
19. Maruyama T, Rodi W, Maruyama Y, Hiraoka H. Large eddy simulation of the turbulent boundary layer behind roughness elements using an artificially generated inflow. *Journal of Wind Engineering and Industrial Aerodynamics* 1999; **83**:381–392.
20. Iizuka S, Murakami S, Tsuchiya N, Mochida A. LES of flow past 2D cylinder with imposed inflow turbulence. *Wind Engineering* 1999; **2**:1291–1298.
21. Stanley SA, Sarkar S, Mellado JP. A study of the flow-field evolution and mixing in a planar turbulent jet using direct numerical simulation. *Journal of Fluid Mechanics* 2002; **450**:377–407.
22. Smirnov A, Shi S, Celik I. Random flow generation technique for large eddy simulations and particle-dynamics modeling. *Journal of Fluids Engineering* 2001; **123**:359–371.
23. Kondo K, Tsuchiya M. Generation of inflow turbulent boundary layer for LES computation. *Wind and Structures* 2002; **4**(2–4):209–226.
24. Batchelor GK. *The Theory of Homogeneous Turbulence*. Cambridge University Press: Cambridge, 1954.
25. Hoshiya M. Simulation of multi-correlated random processes and application to structural vibration problems. *Proceedings of JSCE*, vol. 204, 1972; 121–128.
26. Shinozuka M. Simulation of multivariate and multidimensional random processes. *The Journal of the Acoustical Society of America* 1972; **49**(1):357–367.
27. Klein M, Sadiki A, Janicka J. A digital filter based generation of inflow data for spatially developing direct numerical or large eddy simulations. *Journal of Computational Physics* 2003; **186**:652–665.
28. Kempf A, Klein M, Janicka J. Efficient generation of initial- and inflow conditions for transient turbulent flows in arbitrary geometries. *Flow*, *Turbulence and Combustion* 2005; **74**(1):67–84.
29. Mare LD, Klein M, Jones WP, Janicka J. Synthetic turbulence inflow conditions for large eddy simulation. *Physics of Fluids* 2006; **18**:1–11.
30. Schumacher J. Derivative moments in stationary homogeneous shear turbulence. *Journal of Fluid Mechanics* 2001; **441**:109–118.
31. Rogers MM, Moin P. The structure of the vorticity field in homogeneous turbulent flows. *Journal of Fluid Mechanics* 1985; **176**:33–66.

DOI: 10.1002/fld

32. Pope SB. Stochastic Lagrangian models of velocity in homogeneous turbulent shear flow. *Physics of Fluids* 2002; **14**(5):1696–1702.
33. Sawford BL, Yeung PK. Lagrangian statistics in uniform shear flow: direct numerical simulation and Lagrangian stochastic models. *Physics of Fluids* 2001; **13**(9):2627–2634.
34. Pope SB. *Turbulent Flows*. Cambridge University Press: Cambridge, 2000.
35. Davidson PA. *Turbulence*. Oxford University Press: Oxford, 2004.
36. Townsend AA. *The Structure of Turbulent Shear Flow*. Cambridge University Press: Cambridge, 1975.
37. Gualtieri P, Casciola CM, Benzi R, Amati G, Piva R. Scaling laws and intermittency in homogeneous shear flow. *Physics of Fluids* 2002; **14**:583–596.
38. Hartel C, Kleiser L, Unger F, Friedrich R. Subgrid-scale energy transfer in the near-wall region of turbulent flows. *Physics of Fluids* 1994; **6**:3130–3143.
39. Freitag M, Klein M. Direct numerical simulation of a recirculating, swirling flow. *Flow*, *Turbulence and Combustion* 2005; **75**:51–66.
40. Bonnet J, Moser R, Rodi W. *AGARD Advisory Report 345*, *A Selection of Test Cases for the Validation of Large Eddy Simulations of Turbulent Flows*. AGARD, France, 1998; 91.

DOI: 10.1002/fld